Plasma Membrane Phylloquinone Biosynthesis in Nonphotosynthetic Parasitic Plants

Xi Gu[a], Ing-Gin Chen[b], Scott A. Harding[b,c,d], Batbayar Nyamdari[b,c,d], Maria A. Ortega[b,c,d], Kristen Clermont[e], James H. Westwood[e], Chung-Jui Tsai[a,b,c,d]

[a]Institute of Bioinformatics, University of Georgia, Athens, GA 30602, USA.
[b]School of Forestry and Natural Resources, University of Georgia, Athens, GA 30602, USA.
[c]Department of Genetics, University of Georgia, Athens, GA 30602, USA.
[d]Department of Plant Biology, University of Georgia, Athens, GA 30602, USA.
[e]School of Plant and Environmental Sciences, Virginia Polytechnic Institute and State University, Blacksburg, VA 24061, USA.
Corresponding author: cjtsai@uga.edu

Abstract

Phylloquinone is a lipophilic naphthoquinone found predominantly in chloroplasts and best known for its function in photosystem I electron transport and disulfide bridge formation of photosystem II subunits. Phylloquinone has also been detected in plasma membrane preparations of heterotrophic tissues with potential transmembrane redox function, but the molecular basis for this noncanonical pathway is unknown. Here we provide evidence of plasma membrane phylloquinone biosynthesis in a nonphotosynthetic holoparasite *Phelipanche aegyptiaca*. A nonphotosynthetic and nonplastidial role for phylloquinone is supported by transcription of phylloquinone biosynthetic genes during seed germination and haustorium development, by plasma membrane-localization of alternative terminal enzymes, and by detection of phylloquinone in germinated seeds. Comparative gene network analysis with photosynthetically competent parasites revealed a bias of *Phelipanche* phylloquinone genes toward coexpression with oxidoreductases involved in plasma membrane electron transport. Genes encoding the plasma membrane phylloquinone pathway are also present in several photoautotrophic taxa of Asterids, suggesting an ancient origin of multifunctionality. Our findings suggest that nonphotosynthetic holoparasites exploit alternative targeting of phylloquinone for transmembrane redox signaling associated with parasitism.

Introduction

Phylloquinone (vitamin K1) is a membrane-bound naphthoquinone derivative known to function as an essential electron acceptor in photosystem I (PSI) (Brettel et al., 1986). Phylloquinone also serves as an electron carrier for protein disulfide bond formation crucial for PSII assembly (Furt et al., 2010; Karamoko et al., 2011; Lu et al., 2013). Accordingly, phylloquinone is found predominantly in thylakoids, and most phylloquinone-deficient *Arabidopsis thaliana* mutants are seedling-lethal or growth-impaired (reviewed in Gilles et al., 2016). A sizable phylloquinone pool is stored in plastoglobules attached to thylakoid membranes (Lohmann et al., 2006; Eugeni Piller et al., 2012). A small portion of leaf phylloquinone is present as fully-reduced quinol, with potential redox function during senescence or dark growth (Oostende et al., 2008).

The eubacterial cognate menaquinone (vitamin K2) functions in respiratory electron transport across the cell membrane (Nowicka and Kruk, 2010). A similar role for phylloquinone in plant plasma membrane (PM) electron transport has also been proposed, and phylloquinone has been detected in PM preparations of maize roots (Lüthje et al., 1998; Lochner et al., 2003). UV-irradiation of cultured carrot cells destroyed phylloquinone, and blocked transmembrane electron transport until restoration by phylloquinone feeding (Barr et al., 1992). The PM redox activities can be inhibited by phylloquinone antagonists, dicumarol and warfarin, whereas applications of menadione (vitamin K3) or phylloquinone restored transmembrane electron flow (Döring et al., 1992a; Döring et al., 1992b; Lüthje et al., 1992). Despite these early reports, however, molecular evidence that directly supports PM-targeting of phylloquinone remains elusive.

The phylloquinone biosynthetic pathway has an endosymbiotic origin, comprising a series of "Men" proteins named after their eubacterial homologs (Figure 1). A notable exception is the penultimate enzyme (step 9, Figure 1A) of the flavin-containing NAD(P)H quinone oxidoreductase (FQR/NQR/QR) family recently shown to be necessary for phylloquinone biosynthesis in plants and cyanobacteria (Eugeni Piller et al., 2011; Fatihi et al., 2015). The corresponding enzyme in *A. thaliana*, type II NAD(P)H dehydrogenase C1 (NDC1), was first identified as a mitochondrial respiratory chain component (Michalecka et al., 2003), but later was also found to be targeted to the chloroplast (Carrie et al., 2008), with additional functions in

plastoquinone reduction and redox cycling of α-tocopherols in plastoglobules (Eugeni Piller et al., 2011). Intracellular compartmentalization is a hallmark of phylloquinone biosynthesis, with the early (steps 1-4, Figure 1A) and late pathway steps (8-10) occurring in chloroplasts, and the intermediate steps (5-7) in peroxisomes (Babujee et al., 2010). Even within the chloroplast, the three terminal steps shuttle between envelope membranes (MenA, Schultz et al., 1981), plastoglobules (NDC1, Eugeni Piller et al., 2011), and thylakoid membranes (MenG, Kaiping et al., 1984), highlighting the complex trafficking involved in this pathway.

We have observed in multiple photosynthetic taxa that phylloquinone-specific genes such as *MenA* and *MenG* have measurable expression in heterotrophic tissues where photosynthetic genes are barely detected. To ascertain a noncanonical phylloquinone pathway, we exploited parasitic plants as a photosynthesis-free study system. Among angiosperm parasite families, only the Orobanchaceae contains species that span the full spectrum of photosynthetic capacities, and for which rich transcriptomic resources are available (Westwood et al., 2010; Yang et al., 2015). Of particular interest are obligate holoparasites, such as *Phelipanche aegyptiaca*, that are devoid of photosynthetic activity and obtain all of their carbon from their hosts. In contrast, obligate (*e.g.*, *Striga hermonthica*) and facultative (*e.g.*, *Triphysaria versicolor*) hemiparasites are partially or fully photosynthetic. Here, we report on the biosynthesis and PM targeting of phylloquinone in the nonphotosynthetic *Phelipanche aegyptiaca*. Gene network analysis revealed a strong link between phylloquinone and cellular oxidation-reduction processes implicated in parasitic invasion and haustorium development. We propose that parasitic plants exploit alternative phylloquinone targeting for PM redox regulation associated with parasitism.

Results

P. aegyptiaca contains the full complement of phylloquinone biosynthetic genes

Phylloquinone pathway protein sequences of *Mimulus guttatus*, a photoautotroph from Phrymaceae sister to Orobanchaceae, were searched against transcript assemblies available from the Parasitic Plant Genome Project (Yang et al., 2015). Full-length coding sequences were identified for *PaICS* and *PaMenE* genes in *P. aegyptiaca*, along with partial assemblies of other

94 phylloquinone pathway genes. Fragmented transcripts may represent nonfunctional relics of genes undergoing degeneration or may reflect technical limitations of *de novo* assembly that
96 prevented identification of the full complement of phylloquinone biosynthetic genes. The recovery of full-length *PaICS* and *PaMenE* transcripts strongly favored the latter scenario.
98

We addressed the fragmented assembly challenge by developing a pipeline called PLAS
100 (Parallelized Local Assembly of Sequences) that combines reference-guided mapping (against the *Mimulus* proteome in this case) with iterative *de novo* assembly for transcriptome
102 reconstruction. When applied to the RNA-seq datasets of parasitic plants, we successfully recovered full-length transcripts with intact ORFs for all known phylloquinone genes from the
104 holoparasite (Supplemental Dataset 1). These transcripts were detected at moderate to high levels during *P. aegyptiaca* development, except *PaNDC1*—the latest addition to the pathway—which
106 was poorly expressed (FPKM<10) throughout the holoparasite (Figure 1B). *PHYLLO*, *MenE* and *DHNAT* transcripts were detected at similar levels in the three parasites. In contrast, the
108 expression patterns of *ICS*, *MenB*, *MenA* and *MenG* differed between *P. aegyptiaca* and its photosynthetic relatives *S. hermonthica* and *T. versicolor*, especially in response to germination
110 stimulants and haustorium-inducing factors (HIFs) during early development (Stages 1-3, Figure 1B). However, the apparent lack of *PaNDC1* expression weakened support for a functioning
112 phylloquinone pathway. Alternatively, retention and expression of the other seven phylloquinone pathway genes may point to a different pathway configuration at the penultimate step in the
114 holoparasite.

116 We therefore sought to substantiate phylloquinone production in *P. aegyptiaca*, focusing on early development prior to host exposure and haustorium initiation to avoid potential contamination
118 from the photosynthetic host. HPLC analysis confirmed the presence of phylloquinone in germinated *P. aegyptiaca* seeds (Figure 1C), with an estimated level of 0.05±0.02 pmol/mg dry
120 weight (n=3). For reference, phylloquinone levels in *A. thaliana* seeds were 0.12±0.03 pmol/mg dry weight (n=3) (Figure 1D). The result lent support to phylloquinone biosynthesis in the
122 holoparasite. We next examined other candidates that could participate in the reduction of demethylphylloquinone at the penultimate step (step 9). Besides the multifunctional NDC1
124 (Fatihi et al., 2015), menadione-reducing activities have been demonstrated for two other groups

of evolutionarily conserved QR, one represented by *T. versicolor* TvQR2 (Wrobel et al., 2002)
126 and *A. thaliana* AtFQR1 (Laskowski et al., 2002) of the type IV family (Patridge and Ferry,
2006), and the other by soybean (*Glycine max*) GmNQR of the DT-diaphorase type (Schopfer et
128 al., 2008). *PaNQR* transcripts were detected at moderate levels throughout *P. aegyptiaca*
development (Figure 1B), but they were not coexpressed with any phylloquinone pathway genes
130 (see below). By contrast, *PaQR2* was well expressed during early stages of *P. aegyptiaca*
development like other phylloquinone genes (Figure 1B). Type IV QR2 has in fact been
132 implicated in two-electron reduction of menaquinone and phylloquinone to their respective
quinols in the manually curated KEGG reference pathways (Kanehisa et al., 2018). The
134 structural similarity between phylloquinone and its demethylated precursor, and the reported
substrate promiscuity of the orthologous TvQR2 (Wrobel et al., 2002) lent further support to
136 PaQR2 involvement in the penultimate step of *P. aegyptiaca* phylloquinone biosynthesis.

138 **Phylloquinone biosynthesis is redirected to the plasma membrane in the holoparasite**
Identification of the phylloquinone pathway in *P. aegyptiaca* with vestigial plastids raised the
140 possibility that the biosynthetic enzymes exhibit alternative targeting with nonplastidial
function(s). Protein subcellular localization analyses predicted plastid- and peroxisome-targeting
142 of early (PaICS and PaPHYLLO) and intermediate (PaMenE, PaMenB and PaDHNAT) pathway
steps, respectively, similar to their orthologs in photoautotrophic taxa (Supplemental Table S1
144 and Supplemental Figures S1-S3). However, the predicted polypeptides of late pathway steps
PaMenA and PaMenG are truncated at the N-terminus relative to their photoautotrophic
146 orthologs (Figure 2) and scored poorly for plastid-targeting with multiple prediction programs
(Figure 2A, Supplemental Figures S4 and S5). The N-truncation of PLAS-derived *PaMenA* and
148 *PaMenG* transcripts was independently confirmed by RT-PCR cloning and sequencing
(GenBank accession numbers MT506520 and MT506521), and by identification of N-truncated
150 orthologs from other species (see below).

152 PaMenA is predicted as an integral protein with eight transmembrane helices in a topology
similar to that of AtMenA (Figure 2B). The absence of an N-terminal plastid-targeting peptide in
154 PaMenA suggests its localization to other cellular membranes. The penultimate PaQR2, like its
photoautotrophic orthologs, also lacks plastid-targeting sequence (Supplemental Figures S6),

156 which contrasts with the alternative NDC1s that are predicted plastidial (Supplemental Table
S1). Indeed, PM-association has been reported for *A. thaliana*, rice (*Oryza sativa*) and yeast
158 (*Candida albicans*) QR2 orthologs (Marmagne et al., 2004; Natera et al., 2008; Li et al., 2015).
These data suggest the post-peroxisomal steps are likely targeted to PM in *P. aegyptiaca*. We
160 generated stably transformed *Nicotiana benthamiana* expressing *35S:PaMenA-GFP* or
35S:PaMenG-GFP along with a PM marker *35S:AtPIP2A-mCherry* (Nelson et al., 2007).
162 Confocal imaging showed co-localization of PaMenA and PaMenG with the PM marker in
transgenic roots (Figure 2C-D), providing experimental support for alternative targeting of the
164 N-truncated PaMenA and PaMenG in *P. aegyptiaca*.

166 **The plasma membrane pathway has canonical activity and an ancient origin**

The absence of the N-terminal transit signal is not expected to impact (mature) enzyme catalysis.
168 Using PaMenG as a test case, we performed complementation experiments with the *E. coli*
Δ*menG* mutant strain JW5581 (Baba et al., 2006). The *E. coli* MenG, also called UbiE, is a dual
170 C-methyltransferase involved in both menaquinone and ubiquinone biosynthesis, and its
mutation leads to over-accumulation of demethylmenaquinone (Lee et al., 1997). Constitutive
172 expression of *PaMenG* in the mutant strain restored menaquinone production similar to the *E.*
coli EcMenG-complemented control (Figure 2E). The data provide biochemical evidence for
174 canonical activity of the N-truncated PaMenG.

176 Interestingly, distinct *MenG1* and *MenG2* genes encoding long (plastidial) and short (PM)
isoforms, respectively, are present in both *S. hermonthica* and *T. versicolor* (Figure 2A),
178 suggesting the PM phylloquinone pathway may have evolved before the transition to parasitism.
To strengthen this finding, we mined the One Thousand Plant Transcriptomes (1KP) database
180 (Leebens-Mack et al., 2019) and identified several photoautotrophic species—all from
Lamiales—that harbor both long and short isoforms of MenA and/or MenG, including
182 *Lindenbergia philippensis*, *Rehmannia glutinosa* and *Verbascum thapsus*. In contrast, only N-
truncated short isoforms were found in two other Orobanchaceae holoparasites, *Orobanche*
184 *fasciculata* and *Conopholis americana* (Supplemental Figures S4-S5). Phylogenetic analysis
clustered the plastidial and PM isoforms into distinct groups for both MenA and MenG (Figure
186 2F-G), suggesting their origin from lineage-specific duplication events (hereafter, the PM-

localized short isoforms are referred to as MenA2 and MenG2). Of note, transcripts encoding
188 PM-targeted MenG2 were detected at higher levels than those encoding plastidial MenG1 in both *S. hermonthica* and *T. versicolor* (Figure 1B), suggesting divergent regulation of the two MenG
190 isoforms in photosynthetic hemiparasites.

192

Photosynthetic and nonphotosynthetic parasites exhibit distinct phylloquinone gene
194 **coexpression patterns**

We detected high levels of coexpression among phylloquinone genes in the holoparasites,
196 reminiscent of the patterns observed in photosynthetic taxa, including *T. versicolor* (Figure 3) (except for *A. thaliana AtICSs* and *AtDHNATs* involved in salicylic acid biosynthesis (Garcion et
198 al., 2008) and peroxisomal β-oxidation (Cassin-Ross and Hu, 2014), respectively). Interestingly, early- and late-pathway genes showed distinct coexpression patterns in the obligate hemiparasite
200 *S. hermonthica*, perhaps indicative of dual involvement of those genes in plastidial and nonplastidial functions. To shed light on PM-phylloquinone functions, we extracted the top 500
202 most highly-correlated transcripts for each phylloquinone gene except the alternative *QR2* and *NDC1*. The union set contained 2447, 3677 and 3930 unique transcripts for *P. aegyptiaca*, *S.*
204 *hermonthica* and *T. versicolor*, respectively. Interestingly, *QR2* but not *NDC1* was captured in all three networks. The smaller *P. aegyptiaca* gene set is consistent with stronger coexpression of
206 phylloquinone genes when compared to *S. hermonthica* and *T. versicolor* (Figure 3A-C). Subsets of Gene Ontology (GO)-annotated (Biological Process) transcripts (645, 1199 and 1173 for *P.*
208 *aegyptiaca*, *S. hermonthica* and *T. versicolor*, respectively) were then subjected to functional enrichment analysis. Transcripts associated with 'photosynthesis' comprised 3-4% of the GO-
210 annotated transcripts in photosynthetic parasites but were negligible in *P. aegyptiaca* (Figure 3G). In contrast, transcripts associated with 'oxidation-reduction process', 'protein
212 phosphorylation' and 'defense response' were more enriched in *P. aegyptiaca* relative to *S. hermonthica* and *T. versicolor* (Figure 3G).

214

We focused on transcripts assigned to oxidation-reduction, defense and photosynthesis GO terms
216 for coexpression network analysis. Inclusion of orthologs from all three parasites resulted in 359, 544 and 559 non-redundant transcripts from *P. aegyptiaca*, *S. hermonthica* and *T. versicolor*,

218 respectively (Supplemental Dataset 2). Network visualization of coexpression patterns revealed striking differences (Figure 4). Two dense modules were detected for photosynthetic *S.*
220 *hermonthica* and *T. versicolor*; one enriched with photosynthesis genes (Figure 4A, green nodes) and the other containing known parasitism genes (blue, magenta and cyan nodes, see below).
222 However, only one dense module containing parasitism genes was detected for the holoparasite. The phylloquinone genes (orange nodes) were highly interconnected with parasitism genes in the
224 *P. aegyptiaca* network but were scattered over the two modules in *S. hermonthica* and *T. versicolor* networks, presumably reflecting dual functionality in these taxa. We ranked genes by
226 the number of edges they shared with phylloquinone genes (referred to as k_{PhQ}) in each network and observed a strong enrichment of phylloquinone-interconnected genes in the smaller *P.*
228 *aegyptiaca* network. More than 23% of *P. aegyptiaca* nodes had a k_{PhQ} =4-6 (*i.e.*, connected with a majority of the seven phylloquinone genes). However, less than 3% of the *S. hermonthica*
230 and *T. versicolor* nodes met the same criterion (k_{PhQ} ≥5 of 9-10 phylloquinone genes), and only 10 and 15% of their respective nodes had a k_{PhQ} ≥4 (Figure 4A, k_{PhQ} bars).
232

P. aegyptiaca phylloquinone gene networks associate parasitism with plasma membrane
234 **redox signaling**

Several oxidoreductases known to be involved in parasitism were captured in the phylloquinone
236 gene network of *P. aegyptiaca*. Root-specific apoplastic/secretory peroxidases (PRXs or POXs), including *S. asiatica* SaPOXA and SaPOXB and *P. ramosa* PrPOX1 and PrPRX1, have
238 established roles in haustorium induction via generation of reactive oxygen species (ROS) and oxidation of host cell wall-derived phenolics as HIFs (Kim et al., 1998; González-Verdejo et al.,
240 2006; Veronesi et al., 2007). The *PRX* orthologs (Figure 4B, blue clade) were abundantly expressed in *P. aegyptiaca* throughout seed germination and haustorium development (Figure
242 4C). The phylloquinone-coexpression strength (k_{PhQ}) was highest in *P. aegyptiaca*, followed by *S. hermonthica*, but was not observed for *T. versicolor PRXs*, or for homologs in the neighboring
244 clade of the phylogenetic tree (Figure 4B-C). Thus, the phylloquinone-coexpression strength of the secretory PRXs appears to be positively correlated with parasitism.
246

Also implicated in parasitism are QR1 and QR2, depending on the species. QR1 is a chloroplast
248 envelope protein of the ζ-crystalline type NAD(P)H oxidoreductase family involved in

haustorium development of *T. versicolor* (Bandaranayake et al., 2010). However, haustorium
250 formation in *Phtheirospermum japonicum* involves QR2 (Ishida et al., 2017). Accordingly, *QR2* but not *QR1* is responsive to HIFs in *S. asiatica* and *Phtheirospermum japonicum* (Ishida et al.,
252 2016; Liang et al., 2016), similar to the patterns observed for *P. aegyptiaca* and *S. hermonthica* (Figure 1B). *QR1* was not coexpressed with phylloquinone genes, whereas the phylloquinone-
254 coexpression strength of *QR2* is positively correlated with parasitism like the secretory PRXs. These results support a link between phylloquinone biosynthesis and parasitism.
256

We next searched the *P. aegyptiaca* phylloquinone subnetwork for redox proteins known to
258 participate in transmembrane electron transport (Bérczi and Møller, 2000; Keyes et al., 2000). Several flavocytochrome *b* superfamily proteins are known to catalyze PM electron transport
260 from cytosolic NAD(P)H to apoplastic acceptors, including NAD(P)H oxidases (NOX, also known as respiratory burst oxidase homologs) and ferric reductase oxidases (FRO) (Bérczi and
262 Møller, 2000; Jain et al., 2014). The *P. aegyptiaca* transcriptome lacked *NOX*, but contained an *FRO* (*PaFRO1*) orthologous to *AtFRO4/AtFRO5* tandem duplicates that function as Cu-specific
264 reductases at the root surface (Bernal et al., 2012). *PaFRO1* transcript levels were highest in prehaustorial and haustorial tissues (Figure 4D), consistent with potential involvement in the PM
266 redox system. Interestingly, *S. hermonthica* harbors a *NOX*, but not *FRO*, perhaps indicative of lineage-specific transcriptome rewiring. Its counterpart in *S. asiatica* (*SaNOX1*) is indeed root-
268 specific and HIF-responsive (Liang et al., 2016).

270 Electron transport chains are major sources of ROS which are tightly controlled by antioxidant systems, such as Cu/Zn superoxide dismutases (Cu/Zn-SOD or CDS) and glutathione
272 peroxidases (GPX) (Mittler et al., 2004; Margis et al., 2008). *P. aegyptiaca PaCSD1* (k_{PhQ} =4) and *PaGPX4* (k_{PhQ} =6) were highly coexpressed with phylloquinone genes (Figure 4E-F). CSD1
274 is a known leaderless secretory protein frequently detected in apoplastic/secreted proteomes (Cheng et al., 2009; Pechanova et al., 2010), while GPX4 orthologs in *A. thaliana* (*AtGPX4/5*
276 genome duplicates) were recently shown to be PM-anchored based on redox-sensitive GFP fusions (Attacha et al., 2017). Thus, besides the secretory PaPRXs, PaCSD1 and PaGPX4 may
278 also participate in apoplastic redox modulation in the holoparasite. By contrast, the phylloquinone genes of photosynthetic parasites were coexpressed with gene family members

280 specifically targeted to plastids (orthologs of AtCSD2 and/or Fe-SOD AtFSD2/3), mitochondria
(AtGPX6) or cytosol (AtGPX8; Supplemental Dataset 2). The differential coordination between
282 *P. aegyptiaca* and its photosynthetic relatives with distinct subcellular antioxidant systems is
consistent with their contrasting photosynthetic capabilities, and with a prominent role of
284 phylloquinone in PM redox homeostasis of the nonphotosynthetic holoparasite.

286

Discussion

288

An ancient origin of flexible phylloquinone biosynthesis and targeting

290 We present multiple lines of transcriptional, protein subcellular localization, enzymatic, and
metabolic evidence to support extraplastidial phylloquinone biosynthesis in the
292 nonphotosynthetic *P. aegyptiaca*. Our data further revealed the post-peroxisomal steps as key to
flexible phylloquinone biosynthesis (Figure 5). Alternative targeting to the PM is facilitated by
294 N-truncated MenA2 and MenG2 in conjunction with QR2. QR2 has previously been shown to
function in mitigating oxidative stress in bacteria, yeast and plants (Laskowski et al., 2002;
296 Wrobel et al., 2002; Patridge and Ferry, 2006; Li et al., 2015). In plants, *QR2s* exhibit root-
biased expression and are highly responsive to auxins and quinones, including HIFs in the case
298 of parasitic plants (Matvienko et al., 2001; Laskowski et al., 2002; Ishida et al., 2017) (Figure
1B). The proposed QR2 involvement in PM phylloquinone biosynthesis thus represents another
300 example of a multi-functional NAD(P)H oxidoreductase for the penultimate step, analogous to
NDC1 in plastidial phylloquinone biosynthesis (Fatihi et al., 2015).

302

PM-localized MenA2 and MenG2 likely arose from their plastidial counterparts via gene
304 duplication in the common ancestor of Lamiales (Figure 5). Both *MenA* and *MenG* duplicates are
present in *Lindenbergia* and *Rehmannia*, two nonparasitic genera sister to the parasitic
306 Orobanchaceae (McNeal Joel et al., 2013). However, the evolutionary fate of the duplicates
varied among parasitic lineages with different photosynthetic capabilities (Figure 5). The
308 holoparasitic *P. aegyptiaca*, *Orobanche fasciculata* and *Conopholis americana* have dispensed
with *MenA1* and *MenG1* along with the photosynthetic machinery, retaining only *MenA2* and
310 *MenG2*. On the other hand, the photosynthetic *T. versicolor* and *S. hermonthica* have lost *MenA2*

but retain the *MenG1/2* duplicate, as confirmed in the recently released *S. asiatica* genome
312 (Yoshida et al., 2019). In both *T. versicolor* and *S. hermonthica*, the PM-targeted MenG2 became the dominantly expressed isoform over the plastidial MenG1 (Figure 1B), which was
314 subsequently lost in multiple holoparasites. The data suggest expression divergence of the two phylloquinone pathways in the hemiparasites that predated emergence of holoparasites.
316

An outstanding question in PM phylloquinone biosynthesis regards the co-substrate for MenA-
318 mediated prenylation. In photoautotrophs, the prenyl precursor of plastidial prenylquinones is phytyl-diphosphate derived from geranylgeranyl-diphosphate via *de novo* synthesis or from
320 phytol released upon chlorophyll degradation (Keller et al., 1998; Ischebeck et al., 2006). In *A. thaliana*, the chlorophyll salvage pathway is indispensable for leaf tocopherol and phylloquinone
322 synthesis, but seeds depend on a distinct phytol pool of as-yet-undefined origin (Valentin et al., 2006; Zhang et al., 2014; Wang et al., 2017). *Phelipanche* and related *Orobanche* seeds are filled
324 with protein and oil bodies (Joel et al., 2012), and lipids are the main storage reserve comprising up to 30% of dry seed mass (Bar-Nun and Mayer, 2002). Whether the prenyl moiety of PM
326 phylloquinone is supplied by the cytosolic isoprenoid pathway or via other mechanisms requires further investigation.
328

Phylloquinone involvement in PM redox modulation

330 Involvement of phylloquinone in PM electron transport has been proposed by multiple research groups, based on feeding experiments (Barr et al., 1992; Döring et al., 1992a) and on detection of
332 phylloquinone and QR activities in PM preparations of maize roots and soybean hypocotyls (Lüthje et al., 1998; Bridge et al., 2000; Schopfer et al., 2008). This noncanonical function,
334 however, has not gained widespread acceptance owing to concern over potential organellar contamination in the PM preparations from heterotrophic tissues (Oostende et al., 2008), and to
336 the unexplained biosynthetic origin of PM phylloquinone, until now.

338 The *P. aegyptiaca* phylloquinone network comprised redox proteins typical of a transmembrane electron transport chain, including PaQR2, PaFRO1, PaCSD1, PaGPX4 and PaPRXs. PaQR2
340 can function both as a phylloquinone biosynthetic enzyme and an electron transport chain component with demethylphylloquinone or phylloquinone as acceptors. PaFRO1 orthologs have

342 been genetically characterized in *A. thaliana*, and catalyze transmembrane electron transfer associated with Cu(II) reduction in root tips (Bernal et al., 2012). It is worth noting that redox-
344 active Cu is an essential cofactor of several metalloproteins involved in cellular electron transport chains, and Cu proteins play important roles in ROS homeostasis during growth,
346 development and defense (Bérczi and Møller, 2000; Palmer and Guerinot, 2009). This suggests that the transmembrane redox system for Cu homeostasis has been co-opted, along with PM
348 phylloquinone, to support parasitism in *P. aegyptiaca*. PaCSD1, PaGPX4 and PaPRXs likely function synergistically in apoplastic ROS scavenging and signaling associated with PM electron
350 transport. Our data thus provide molecular evidence from parasitic plants to corroborate the long-hypothesized involvement of phylloquinone in PM redox processes in photoautotrophic species
352 (Lüthje et al., 1998; Bérczi and Møller, 2000; Lochner et al., 2003).

354 **A role for PM phylloquinone in redox signaling associated with parasitism**

The early stages of the parasitic lifecycle can be characterized as a continuum of oxidative
356 events, from activation and perception of host HIFs, to induction of haustoria for host penetration and vascular connection (Keyes et al., 2000; Fernández-Aparicio et al., 2016). Redox
358 modulation is also integral to normal growth and development, as well as defense and counter-defense in the case of host-parasite interactions (Kim et al., 1998; Mittler et al., 2004). Redox-
360 active phylloquinone in the PM may function in all of these processes, but most likely in ways specifically associated with haustorium initiation based on network inference and coexpression
362 with known parasitism genes. In the xenognosis model depicted by Keyes et al. (2000), host-derived signals are perceived by a PM-bound electron transport chain for haustorium initiation.
364 Because haustorium signaling shares similar quinone cofactor and redox range requirements with organellar redox circuits (Smith et al., 1996), Keyes et al. (2000) have speculated on the
366 involvement of organelles in the redox relay of haustorium signaling. Our finding that *P. aegyptiaca* exploited phylloquinone from a defunct photosynthetic electron transport chain for
368 PM redox systems is consistent with the model.

370 Comparative analysis of phylloquinone gene coexpression networks recapitulated the evolutionary shifts in photosynthetic competence, decreasing from facultative (*T. versicolor*) and
372 obligate (*S. hermonthica*) hemiparasites to the obligate holoparasite *P. aegyptiaca*. Conversely,

the increasing representation of genes involved in redox processes is positively correlated with
374 the degree of parasitism. This is consistent with the view that some redox-regulated processes in host recognition and haustorium development diversified during the evolution of parasitism
376 (Westwood et al., 2010; Yoshida et al., 2016). *Phelipanche* and related *Orobanche* spp. differ from hemiparasites in many aspects of development and host interactions (Yoshida et al., 2016).
378 For instance, *Phelipanche* and *Orobanche* spp. do not develop the same swollen structure with modified root hairs typical of *S. hermonthica* and *T. versicolor* haustoria, and the haustorium
380 induction chemistry in these holoparasites remains poorly understood (Fernández-Aparicio et al., 2016). Perhaps not surprisingly, taxon-dependent coordination between phylloquinone genes and
382 redox proteins was evident. Phylloquinone-coexpression with chloroplastic ROS scavengers in the hemiparasites is consistent with retention of the plastidial pathway for photosynthetic
384 electron transport. The coordination between components of PM phylloquinone electron transport chain and apoplastic ROS metabolism in *P. aegyptiaca* again attests to the increased
386 specialization of signaling mechanisms associated with holoparasitism.

388 In closing, the previously proposed involvement of phylloquinone in PM electron transport gains molecular support in this study. Our work highlights a novel link between PM phylloquinone and
390 parasitism that warrants future experimental verification. Repurposing phylloquinone for PM redox signaling associated with haustorium development thus adds to documented evolutionary
392 innovation of parasitic plants. The existence of the alternative pathway in nonparasitic lamiales should also motivate research into the functions of PM phylloquinone in photoautotrophic
394 species.

396

398 **Methods**

400 **Transcriptome assembly of parasitic plants**

RNA-Seq data of *P. aegyptiaca*, *S. hermonthica* and *T. versicolor* were downloaded from the
402 Parasitic Plant Genome Project database (http://ppgp.huck.psu.edu/). After quality control filtering, cleaned reads were assembled using the custom PLAS pipeline. Briefly, PLAS

404 performs reference-guided read mapping using Bowtie 2 v2.2.3 (Langmead and Salzberg, 2012)
against the closely related *Mimulus guttatus* proteome binned by homology to facilitate parallel
406 computing. Mapped reads were used for *de novo* assembly by Trinity (Haas et al., 2013), and
the assembled contigs were quality-checked against the reference in each bin by Blast before
408 being used as baits in the next round of *de novo* assembly. This process was repeated for up to
10 iterations until the output was stable. Assembled sequences were filtered to remove potential
410 contaminations (*e.g.*, host plants, protozoa, invertebrates, bacteria, fungi and human sequences)
and redundant contigs sharing ≥95% sequence identity. The transcriptome was annotated against
412 *A. thaliana* and *M. guttatus* proteomes and UniProt database. Transcript abundance was
estimated using eXpress 1.5.1 (Roberts and Pachter, 2013). Additional *MenA* and *MenG*
414 sequences were obtained from the 1KP database (https://db.cngb.org/onekp) by BlastN against
the Core Eudicots/Asterids clade using *P. aegyptiaca* sequences as query. The assembled
416 transcriptome sequences of parasitic plants, the PLAS pipeline and other codes are available at
https://github.com/TsailabBioinformatics/PM-PhQ. All phylloquinone and relevant transcripts
418 described in this work were manually curated (Supplemental Dataset S1). *PaMenA2* and
PaMenG2 were further confirmed by RT-PCR. Briefly, cRNA derived from RNA isolated from
420 stages 2 and 3 as described in Yang et al. (2015) was reverse transcribed using SuperScript™ IV
reverse transcriptase (Invitrogen) with mixed random hexamers and gene-specific reverse
422 primers (Supplemental Table S2). PCR was performed using Q5 High-Fidelity DNA Polymerase
(NEB) with gene-specific primers (Supplemental Table 2), column purified for Gibson assembly
424 into pUC19 using NEBBuilder® HiFi DNA Assembly Master Mix, and confirmed by Sanger
sequencing (Eurofins Genomics).
426

Subcellular and transmembrane domain prediction and gene structure

428 Phylloquinone gene sequences of photosynthetic species were downloaded from Phytozome v11.
Subcellular localization was predicted by Predotar 1.04 (Small et al., 2004), TargetP 1.1
430 (Emanuelsson et al., 2007), Protein Prowler 1.2 (Bodén and Hawkins, 2005), and WolF PSORT
(Horton et al., 2007). Transmembrane domain was predicted by TMHMM Server v.2.0 (Krogh et
432 al., 2001), and data plotted in *R*. Gene structures were drawn by Gene Structure Display Server
2.0 (Hu et al., 2015). The exon-intron junctions of parasitic *MenA* and *MenG* were inferred by
434 Blast alignment of transcripts against genomic short read data of *P. aegyptiaca* (NCBI Sequence

Read Archive accession SRX2067908), *S. hermonthica* (SRX2067907) and *T. versicolor*.
436 Sequence alignment was performed using MUSCLE 3.8.31 (Edgar, 2004) and visualized with Color Align Conservation (www.bioinformatics.org/sms2/color_align_cons.html).
438

Coexpression analysis

440 Transcripts with an FPKM ≥2 in at least two samples were subject to pair-wise Gini Correlation Coefficient (GCC) computation using a python script. Phylloquinone-coexpressed transcripts
442 were defined as the 500 most highly correlated transcripts or those with a GCC ≥0.8 for each phylloquinone gene, excluding the alternative *NDC1* and *QR2*. The union sets were subjected to
444 Gene Ontology enrichment analysis using topGO 2.26.0 (Alexa et al., 2006). To facilitate comparative analysis between species, ortholog groups were constructed by OrthoFinder 1.0.8
446 (Emms and Kelly, 2015). Network visualization was performed in Cytoscape 3.4.0 (Shannon et al., 2003) using prefuse force-directed layout, with a GCC cutoff of 0.6.
448

RNA-seq data processing of photoautotrophic species

450 RNA-seq data of *A. thaliana*, *G. max* and *Populus tremula* × *alba* were downloaded from the NCBI SRA and quality control processed by Cutadapt 1.9.dev1 (Martin, 2011) and Trimmomatic
452 0.32 (Bolger et al., 2014). Reads were mapped by Tophat 2.0.13 (Kim et al., 2013), alignment sorted by Samtools 1.2 (Li et al., 2009), and read count and expression estimation obtained by
454 HTseq 0.6.1p1 (Anders et al., 2015) and DESeq2 (Love et al., 2014). *A. thaliana* data used for GCC computation (excluding stressed samples) were SRA236885, SRA091517, SRA269936,
456 SRA219425, SRA308579, SRA050132, SRA067724, SRA291734, SRA269101, SRA098075, SRA100242, SRA122395, SRA163488, SRA064368, SRA246225, SRA248861, SRA202878,
458 SRA201550, SRA303151, SRA221137, SRA272654, and SRA221060. *G. max* data included SRA187830, SRA047293, SRA036577, SRA116533, SRA091756, SRA187830, SRA036538,
460 SRA036577, and SRA129337. *P. tremula* × *alba* datasets were SRA274261 and SRA097208.

462 **Phylogenetic tree construction**

The protein sequences of *P. ramosa* PrPRX1 (AAY89058) and PrPOX1 (AAU04440), and *S.*
464 *asiatica* SaPOXA (AAB97853) and SaPOXB (AF043235) were searched against the PLAS assemblies of *P. aegyptiaca*, *S. hermonthica* and *T. versicolor* to identify orthologs. Their protein

466 sequences were aligned by MUSCLE 3.8.31 (Edgar, 2004) and the alignment trimmed by
Gblocks (Castresana, 2000). Bayesian phylogenetic tree was constructed using MrBayes 3.2.5
468 (Ronquist et al., 2012). Phylogenetic trees for MenA and MenG were similarly constructed using
protein sequences obtained from Phytozome or 1KP followed by manual curation (Supplemental
470 Dataset S1), and visualized by MEGA X (Kumar et al., 2018).

472 **Phylloquinone analysis**

P. aegyptiaca seeds were surface-sterilized, pre-conditioned on moist filter paper for 7-10 days,
474 and treated with GR-24 for 4-6 days before collection of stage 1 germinated seeds as described
(Westwood et al., 2012). Non-imbibed *A. thaliana* (Col-0) seeds were used without further
476 treatment. Tissues were snap-frozen in liquid nitrogen, freeze-dried and milled to a fine powder
for phylloquinone analysis as described (Booth et al., 1994). Tissues were partitioned twice in
478 isopropanol:hexane (3:2 v/v), with menaquinone MK-4 (Sigma V9378) as a reference for *P.*
aegyptiaca analysis. The hexane phase was dried under nitrogen, and resuspended in methylene
480 chloride:methanol (1:4, v/v), 10 mM $ZnCl_2$, 5 mM Na-acetate, and 5 mM acetic acid. Isocratic
reverse-phase HPLC (Agilent Eclipse Plus C18 column, 5 µm, 4.6×250 mm) was carried out
482 using methanol:methylene chloride (9:1, v/v), with post-column Zn reduction and fluorescence
detection (excitation 244 nm, emission 418 nm). Phylloquinone peaks were verified by
484 comparison with the authentic standard (Sigma 47773) and concentrations were estimated using
calibration curves of the standard.

486

***Nicotiana benthamiana* transformation and confocal microscopy**

488 *PaMenA* and *PaMenG* coding sequences were gene-synthesize (General Biosystems) and
subcloned into *Xba*I-digested pCX-AtMenA.1-GFP vector to generate pCX-PaMenA-GFP and
490 pCX-PaMenG-GFP, respectively. The pCX-AtMenA.1-GFP vector was previously constructed
by Gibson assembly of PCR-amplified AtMenA.1 (obtained from Arabidopsis Biological
492 Resource Center) and GFP (from pCXDG) into *Bam*HI-digested pCXSN vector (Chen et al.,
2009) (see Supplemental Table S2 for primers). Due to concern over 35S promoter silencing in
494 co-transformation experiments, another PaMenA-GFP construct was prepared by PCR using
pCX-PaManA-GFP as template and primers containing a viral 2A peptide bridge sequence (Luke
496 et al., 2015) to link the HPT (hygromycin phosphotransferase) coding sequence to PaMenA-GFP

behind double 35S promoter as one transcriptional unit (*35S:PaMenA-GFP-2A-HPT*)
498 (Supplemental Table S2). All constructs were sequence verified. *Agrobacterium*-mediated transformation of *Nicotiana benthamiana* was performed as described and regenerated on
500 selection media (Pathi et al., 2013) using individual constructs (pCX-PaMenA-GFP, pCX-PaMenG-GFP and pCX-AtMenA.1-GFP) or in conjunction with a PM (PIP2A-mCherry) or
502 tonoplast intrinsic protein (γ-TIP-mCherry) marker (Nelson et al., 2007) (pCX-PaMenA-GFP-2A-HPT + AtPIP2A-mCherry, pCX-PaMenA-GFP-2A-HPT + At γ-TIP-mCherry, pCX-
504 PaMenG-GFP + AtPIP2A-mCherry and pCX-PaMenG-GFP + At γ-TIP-mCherry). Root samples from independent transformants were screened under a fluorescence microscope and at least
506 three positive lines were further examined using a Zeiss LSM 880 upright confocal microscope in the Biomedical Microscopy Core at the University of Georgia. GFP signal was detected using
508 an Argon excitation laser (488 nm) and an emission filter at 490-540 nm, and mCherry signal was obtained using a HeNe excitation laser (543 nm) and an emission filter at 547-697 nm.
510

***E. coli* complementation**

512 The *PaMenG2* and *EcMenG* (positive control) coding sequences were PCR-amplified (see Supplemental Table S2 for primers) for Gibson assembly into a constitutive expression vector
514 pUCM (Kim et al., 2010), and transformed into *E. coli* DH5α. Sequence-verified plasmids were transformed into *E. coli* strain JW5581 carrying the mutated *menG* (*ubiE*) gene (obtained from
516 the *E. coli* Genetic Stock Center). At least two PCR-confirmed colonies per construct were used for complementation experiments. Approximately 30 mg of freeze-dried bacterial cells were
518 extracted as described (Booth et al., 1994) using a Misonix sonicator. Reverse-phase HPLC conditions were the same as above except with a run time of 40 min.
520

522 **Supplemental Materials**

Supplemental Table S1. Plastid-targeting prediction for ICS, PHYLLO and NDC1.
524 Supplemental Table S2. List of primers
Supplemental Figure S1. MenE sequence alignment with C-terminal peroxisome targeting signal
526 PTS1.

Supplemental Figure S2. MenB sequence alignment with N-terminal peroxisome targeting signal PTS2.

Supplemental Figure S3. DHNAT sequence alignment with C-terminal peroxisome targeting signal PTS1.

Supplemental Figure S4. MenA sequence alignment.

Supplemental Figure S5. MenG sequence alignment.

Supplemental Figure S6. QR2 sequence alignment.

Supplemental Dataset S1. PLAS-assembled or 1KP-derived and manually curated transcript sequences of phylloquinone biosynthetic and coexpressed genes described in the manuscript.

Supplemental Dataset S2. Lists of transcripts used in coexpression network analysis.

Acknowledgments: We thank L.-J. Xue for the GCC Python script, M. Curley, M. Tsai, N. Rodman, and K.B. Aulakh for laboratory assistance, M.K. Kandasamy for confocal microscopy assistance, and D. Lynn (Emory University) for insightful discussion. This research was supported by Georgia Research Alliance-Hank Haynes Forest Biotechnology Endowment (C.-J.T.), National Science Foundation grants IOS-1444567 (C.-J.T.) and IOS-1238057 (J.H.W.), National Institute of Food and Agriculture grants 2015-67013-22812 (C.-J.T.) and VA-135997 (J.H.W.), and University of Georgia Graduate School's Innovative and Interdisciplinary Research Grant (X.G.).

Author contributions: C.-J.T and X.G. conceived the study; X.G. performed all bioinformatic analyses with contributions from C.-J.T.; I.-G.C. performed bacterial complementation, tobacco transformation and microscopic analyses with help from M.A.O.; S.A.H, B.N., and I.-G.C. performed metabolic analyses; K.C. and J.H.W. contributed materials; X.G. and C.-J.T. wrote the manuscript with input from S.A.H and J.H.W.

References

558 **Alexa, A., Rahnenführer, J., and Lengauer, T.** (2006). Improved scoring of functional groups from gene expression data by decorrelating GO graph structure. Bioinformatics **22,** 1600-
560 1607.

Anders, S., Pyl, P.T., and Huber, W. (2015). HTSeq—a Python framework to work with high-
562 throughput sequencing data. Bioinformatics **31,** 166-169.

Attacha, S., Solbach, D., Bela, K., Moseler, A., Wagner, S., Schwarzländer, M., Aller, I.,
564 **Müller Stefanie, J., and Meyer Andreas, J.** (2017). Glutathione peroxidase-like enzymes cover five distinct cell compartments and membrane surfaces in Arabidopsis
566 thaliana. Plant, Cell & Environment **40,** 1281-1295.

Baba, T., Ara, T., Hasegawa, M., Takai, Y., Okumura, Y., Baba, M., Datsenko, K.A.,
568 **Tomita, M., Wanner, B.L., and Mori, H.** (2006). Construction of *Escherichia coli* K-12 in-frame, single-gene knockout mutants: the Keio collection. Molecular systems biology
570 **2,** 2006.0008-2006.0008.

Babujee, L., Wurtz, V., Ma, C., Lueder, F., Soni, P., van Dorsselaer, A., and Reumann, S.
572 (2010). The proteome map of spinach leaf peroxisomes indicates partial compartmentalization of phylloquinone (vitamin K1) biosynthesis in plant peroxisomes.
574 Journal of Experimental Botany **61,** 1441-1453.

Bandaranayake, P.C.G., Filappova, T., Tomilov, A., Tomilova, N.B., Jamison-McClung, D.,
576 **Ngo, Q., Inoue, K., and Yoder, J.I.** (2010). A single-electron reducing quinone oxidoreductase is necessary to induce haustorium development in the root parasitic plant
578 *Triphysaria*. Plant Cell **22,** 1404-1419.

Bar-Nun, N., and Mayer, A.M. (2002). Composition of and changes in storage compounds in
580 *Orobanche aegyptiaca* seeds during preconditioning. Israel Journal of Plant Sciences **50,** 278-279.

582 **Barr, R., Pan, R.S., Crane, F.L., Brightman, A.O., and Morré, D.J.** (1992). Destruction of vitamin K1 of cultured carrot cells by ultraviolet radiation and its effect on plasma
584 membrane electron transport reactions. Biochemistry International **27,** 449-456.

Bérczi, A., and Møller, I.M. (2000). Redox enzymes in the plant plasma membrane and their
586 possible roles. Plant Cell and Environment **23,** 1287-1302.

Bernal, M., Casero, D., Singh, V., Wilson, G.T., Grande, A., Yang, H., Dodani, S.C.,
588 **Pellegrini, M., Huijser, P., Connolly, E.L., Merchant, S.S., and Krämer, U.** (2012). Transcriptome sequencing identifies SPL7-regulated copper acquisition genes
590 FRO4/FRO5 and the copper dependence of iron homeostasis in *Arabidopsis*. Plant Cell **24,** 738-761.

592 **Bodén, M., and Hawkins, J.** (2005). Prediction of subcellular localization using sequence-biased recurrent networks. Bioinformatics **21,** 2279-2286.

594 **Bolger, A.M., Lohse, M., and Usadel, B.** (2014). Trimmomatic: a flexible trimmer for Illumina sequence data. Bioinformatics **30,** 2114-2120.

596 **Booth, S.L., Davidson, K.W., and Sadowski, J.A.** (1994). Evaluation of an HPLC method for the determination of phylloquinone (vitamin K1) in various food matrixes. Journal of
598 Agricultural and Food Chemistry **42,** 295-300.

Brettel, K., Sétif, P., and Mathis, P. (1986). Flash-induced absorption changes in photosystem I
600 at low temperature: evidence that the electron acceptor A1 is vitamin K1. FEBS Letters **203,** 220-224.

602 **Bridge, A., Barr, R., and Morré, D.J.** (2000). The plasma membrane NADH oxidase of soybean has vitamin K1 hydroquinone oxidase activity. Biochimica et Biophysica Acta
604 (BBA) - Biomembranes **1463,** 448-458.

Carrie, C., Murcha, M.W., Kuehn, K., Duncan, O., Barthet, M., Smith, P.M., Eubel, H.,
606 **Meyer, E., Day, D.A., Millar, A.H., and Whelan, J.** (2008). Type II NAD(P)H dehydrogenases are targeted to mitochondria and chloroplasts or peroxisomes in
608 *Arabidopsis thaliana*. FEBS Letters **582,** 3073-3079.

Cassin-Ross, G., and Hu, J. (2014). Systematic phenotypic screen of *Arabidopsis* peroxisomal
610 mutants identifies proteins involved in β-oxidation. Plant Physiology **166,** 1546-1559.

Castresana, J. (2000). Selection of conserved blocks from multiple alignments for their use in
612 phylogenetic analysis. Molecular Biology and Evolution **17,** 540-552.

Chen, S., Songkumarn, P., Liu, J., and Wang, G.-L. (2009). A versatile zero background T-
614 vector system for gene cloning and functional genomics. Plant Physiol. **150,** 1111-1121.

Cheng, F.-y., Blackburn, K., Lin, Y.-m., Goshe, M.B., and Williamson, J.D. (2009). Absolute
616 protein quantification by LC/MSE for global analysis of salicylic acid-induced plant protein secretion responses. Journal of Proteome Research **8,** 82-93.

618 **Döring, O., Lüthje, S., and Böttger, M.** (1992a). Modification of the activity of the plasma membrane redox system of *Zea mays* L. roots by vitamin K3 and dicumarol. Journal of
620 Experimental Botany **43,** 175-181.

Döring, O., Lüthje, S., and Böttger, M. (1992b). Inhibitors of the plasma membrane redox
622 system of *Zea mays* L. roots. The vitamin K antagonists dicumarol and warfarin. Biochimica et Biophysica Acta (BBA) - Biomembranes **1110,** 235-238.

624 **Edgar, R.C.** (2004). MUSCLE: multiple sequence alignment with high accuracy and high throughput. Nucleic Acids Research **32,** 1792-1797.

626 **Emanuelsson, O., Brunak, S., von Heijne, G., and Nielsen, H.** (2007). Locating proteins in the cell using TargetP, SignalP and related tools. Nat. Protocols **2,** 953-971.

628 **Emms, D.M., and Kelly, S.** (2015). OrthoFinder: solving fundamental biases in whole genome comparisons dramatically improves orthogroup inference accuracy. Genome Biology **16,**
630 157.

Eugeni Piller, L., Abraham, M., Dörmann, P., Kessler, F., and Besagni, C. (2012). Plastid
632 lipid droplets at the crossroads of prenylquinone metabolism. Journal of Experimental Botany **63,** 1609-1618.

634 **Eugeni Piller, L., Besagni, C., Ksas, B., Rumeau, D., Bréhélin, C., Glauser, G., Kessler, F., and Havaux, M.** (2011). Chloroplast lipid droplet type II NAD(P)H quinone
636 oxidoreductase is essential for prenylquinone metabolism and vitamin K_1 accumulation. Proceedings of the National Academy of Sciences **108,** 14354-14359.

638 **Fatihi, A., Latimer, S., Schmollinger, S., Block, A., Dussault, P.H., Vermaas, W.F.J., Merchant, S.S., and Basset, G.J.** (2015). A dedicated type II NADPH dehydrogenase
640 performs the penultimate step in the biosynthesis of vitamin K1 in *Synechocystis* and *Arabidopsis*. Plant Cell **27,** 1730-1741.

642 **Fernández-Aparicio, M., Masi, M., Maddau, L., Cimmino, A., Evidente, M., Rubiales, D., and Evidente, A.** (2016). Induction of haustorium development by sphaeropsidones in
644 radicles of the parasitic weeds *Striga* and *Orobanche*. A structure–activity relationship study. Journal of Agricultural and Food Chemistry **64,** 5188-5196.

646 **Furt, F., Oostende, C.v., Widhalm, J.R., Dale, M.A., Wertz, J., and Basset, G.J.C.** (2010). A bimodular oxidoreductase mediates the specific reduction of phylloquinone (vitamin K1)
648 in chloroplasts. Plant Journal **64,** 38-46.

Garcion, C., Lohmann, A., Lamodiere, E., Catinot, J., Buchala, A., Doermann, P., and
650 **Metraux, J.-P.** (2008). Characterization and biological function of the ISOCHORISMATE SYNTHASE2 gene of Arabidopsis. Plant Physiol. **147,** 1279-1287.

652 **Gilles, J.B., Scott, L., Abdelhak, F., Eric, S., and Anna, B.** (2016). Phylloquinone (Vitamin K1): Occurrence, biosynthesis and functions. Mini-Reviews in Medicinal Chemistry **16,**
654 1-11.

González-Verdejo, C.I., Barandiaran, X., Moreno, M.T., Cubero, J.I., and Di Pietro, A.
656 (2006). A peroxidase gene expressed during early developmental stages of the parasitic plant *Orobanche ramosa*. Journal of Experimental Botany **57,** 185-192.

658 **Haas, B.J., Papanicolaou, A., Yassour, M., Grabherr, M., Blood, P.D., Bowden, J., Couger, M.B., Eccles, D., Li, B., Lieber, M., MacManes, M.D., Ott, M., Orvis, J., Pochet, N.,**
660 **Strozzi, F., Weeks, N., Westerman, R., William, T., Dewey, C.N., Henschel, R., LeDuc, R.D., Friedman, N., and Regev, A.** (2013). *De novo* transcript sequence
662 reconstruction from RNA-Seq: reference generation and analysis with Trinity. Nature protocols **8,** 10.1038/nprot.2013.1084.

664 **Horton, P., Park, K.-J., Obayashi, T., Fujita, N., Harada, H., Adams-Collier, C.J., and Nakai, K.** (2007). WoLF PSORT: protein localization predictor. Nucleic Acids Research
666 **35,** W585-W587.

Hu, B., Jin, J., Guo, A.-Y., Zhang, H., Luo, J., and Gao, G. (2015). GSDS 2.0: an upgraded
668 gene feature visualization server. Bioinformatics **31,** 1296-1297.

Ischebeck, T., Zbierzak, A.M., Kanwischer, M., and Dörmann, P. (2006). A salvage pathway
670 for phytol metabolism in *Arabidopsis*. Journal of Biological Chemistry **281,** 2470-2477.

Ishida, J.K., Yoshida, S., and Shirasu, K. (2017). Quinone oxidoreductase 2 is involved in
672 haustorium development of the parasitic plant *Phtheirospermum japonicum*. Plant signaling & behavior **12,** e1319029-e1319029.

674 **Ishida, J.K., Wakatake, T., Yoshida, S., Takebayashi, Y., Kasahara, H., Wafula, E., dePamphilis, C.W., Namba, S., and Shirasu, K.** (2016). Local auxin biosynthesis
676 mediated by a YUCCA flavin monooxygenase regulates haustorium development in the parasitic plant *Phtheirospermum japonicum*. Plant Cell **28,** 1795-1814.

678 **Jain, A., Wilson, G., and Connolly, E.** (2014). The diverse roles of FRO family metalloreductases in iron and copper homeostasis. Frontiers in Plant Science **5**.

680 **Joel, D.M., Bar, H., Mayer, A.M., Plakhine, D., Ziadne, H., Westwood, J.H., and Welbaum, G.E.** (2012). Seed ultrastructure and water absorption pathway of the root-parasitic plant
682 *Phelipanche aegyptiaca* (Orobanchaceae). Annals of botany **109,** 181-195.

Kaiping, S., Soll, J., and Schultz, G. (1984). Site of methylation of 2-phytyl-1,4-naphthoquinol
684 in phylloquinone (vitamin K1) synthesis in spinach chloroplasts. Phytochemistry **23,** 89-91.

686 **Kanehisa, M., Sato, Y., Furumichi, M., Morishima, K., and Tanabe, M.** (2018). New approach for understanding genome variations in KEGG. Nucleic Acids Research **47,**
688 D590-D595.

Karamoko, M., Cline, S., Redding, K., Ruiz, N., and Hamel, P.P. (2011). Lumen thiol
690 oxidoreductase1, a disulfide bond-forming catalyst, is required for the assembly of photosystem II in Arabidopsis. Plant Cell **23,** 4462-4475.

692 **Keller, Y., Bouvier, F., d'Harlingue, A., and Camara, B.** (1998). Metabolic compartmentation of plastid prenyllipid biosynthesis. European Journal of Biochemistry **251,** 413-417.
694 **Keyes, J.W., O'Malley, C.R., Kim, D., and Lynn, G.D.** (2000). Signaling organogenesis in parasitic angiosperms: Xenognosin generation, perception, and response. Journal of Plant
696 Growth Regulation **19,** 217-231.
Kim, D., Kocz, R., Boone, L., John Keyes, W., and Lynn, D.G. (1998). On becoming a
698 parasite: evaluating the role of wall oxidases in parasitic plant development. Chemistry & Biology **5,** 103-117.
700 **Kim, D., Pertea, G., Trapnell, C., Pimentel, H., Kelley, R., and Salzberg, S.L.** (2013). TopHat2: accurate alignment of transcriptomes in the presence of insertions, deletions
702 and gene fusions. Genome Biology **14,** R36.
Kim, S.H., Park, Y.H., Schmidt-Dannert, C., and Lee, P.C. (2010). Redesign, reconstruction,
704 and directed extension of the Brevibacterium linens C40 carotenoid pathway in Escherichia coli. Applied and environmental microbiology **76,** 5199-5206.
706 **Krogh, A., Larsson, B., von Heijne, G., and Sonnhammer, E.L.L.** (2001). Predicting transmembrane protein topology with a hidden markov model: application to complete
708 genomes1. Journal of Molecular Biology **305,** 567-580.
Kumar, S., Stecher, G., Li, M., Knyaz, C., and Tamura, K. (2018). MEGA X: Molecular
710 Evolutionary Genetics Analysis across computing platforms. Molecular Biology and Evolution **35,** 1547-1549.
712 **Langmead, B., and Salzberg, S.L.** (2012). Fast gapped-read alignment with Bowtie 2. Nature methods **9,** 357-359.
714 **Laskowski, M.J., Dreher, K.A., Gehring, M.A., Abel, S., Gensler, A.L., and Sussex, I.M.** (2002). FQR1, a novel primary auxin-response gene, encodes a flavin mononucleotide-
716 binding quinone reductase. Plant Physiology **128,** 578-590.
Lee, P.T., Hsu, A.Y., Ha, H.T., and Clarke, C.F. (1997). A C-methyltransferase involved in
718 both ubiquinone and menaquinone biosynthesis: isolation and identification of the *Escherichia coli ubiE* gene. Journal of bacteriology **179,** 1748-1754.
720 **Leebens-Mack, J.H., Barker, M.S., Carpenter, E.J., Deyholos, M.K., Gitzendanner, M.A., Graham, S.W., Grosse, I., Li, Z., Melkonian, M., Mirarab, S., Porsch, M., Quint, M.,**
722 **Rensing, S.A., Soltis, D.E., Soltis, P.S., Stevenson, D.W., Ullrich, K.K., Wickett, N.J., DeGironimo, L., Edger, P.P., Jordon-Thaden, I.E., Joya, S., Liu, T., Melkonian, B.,**
724 **Miles, N.W., Pokorny, L., Quigley, C., Thomas, P., Villarreal, J.C., Augustin, M.M., Barrett, M.D., Baucom, R.S., Beerling, D.J., Benstein, R.M., Biffin, E., Brockington,**
726 **S.F., Burge, D.O., Burris, J.N., Burris, K.P., Burtet-Sarramegna, V., Caicedo, A.L., Cannon, S.B., Çebi, Z., Chang, Y., Chater, C., Cheeseman, J.M., Chen, T., Clarke,**
728 **N.D., Clayton, H., Covshoff, S., Crandall-Stotler, B.J., Cross, H., dePamphilis, C.W., Der, J.P., Determann, R., Dickson, R.C., Di Stilio, V.S., Ellis, S., Fast, E., Feja, N.,**
730 **Field, K.J., Filatov, D.A., Finnegan, P.M., Floyd, S.K., Fogliani, B., García, N., Gâteblé, G., Godden, G.T., Goh, F., Greiner, S., Harkess, A., Heaney, J.M.,**
732 **Helliwell, K.E., Heyduk, K., Hibberd, J.M., Hodel, R.G.J., Hollingsworth, P.M., Johnson, M.T.J., Jost, R., Joyce, B., Kapralov, M.V., Kazamia, E., Kellogg, E.A.,**
734 **Koch, M.A., Von Konrat, M., Könyves, K., Kutchan, T.M., Lam, V., Larsson, A., Leitch, A.R., Lentz, R., Li, F.-W., Lowe, A.J., Ludwig, M., Manos, P.S., Mavrodiev,**
736 **E., McCormick, M.K., McKain, M., McLellan, T., McNeal, J.R., Miller, R.E., Nelson, M.N., Peng, Y., Ralph, P., Real, D., Riggins, C.W., Ruhsam, M., Sage, R.F.,**

Sakai, A.K., Scascitella, M., Schilling, E.E., Schlösser, E.-M., Sederoff, H., Servick, S., Sessa, E.B., Shaw, A.J., Shaw, S.W., Sigel, E.M., Skema, C., Smith, A.G., Smithson, A., Stewart, C.N., Stinchcombe, J.R., Szövényi, P., Tate, J.A., Tiebel, H., Trapnell, D., Villegente, M., Wang, C.-N., Weller, S.G., Wenzel, M., Weststrand, S., Westwood, J.H., Whigham, D.F., Wu, S., Wulff, A.S., Yang, Y., Zhu, D., Zhuang, C., Zuidof, J., Chase, M.W., Pires, J.C., Rothfels, C.J., Yu, J., Chen, C., Chen, L., Cheng, S., Li, J., Li, R., Li, X., Lu, H., Ou, Y., Sun, X., Tan, X., Tang, J., Tian, Z., Wang, F., Wang, J., Wei, X., Xu, X., Yan, Z., Yang, F., Zhong, X., Zhou, F., Zhu, Y., Zhang, Y., Ayyampalayam, S., Barkman, T.J., Nguyen, N.-p., Matasci, N., Nelson, D.R., Sayyari, E., Wafula, E.K., Walls, R.L., Warnow, T., An, H., Arrigo, N., Baniaga, A.E., Galuska, S., Jorgensen, S.A., Kidder, T.I., Kong, H., Lu-Irving, P., Marx, H.E., Qi, X., Reardon, C.R., Sutherland, B.L., Tiley, G.P., Welles, S.R., Yu, R., Zhan, S., Gramzow, L., Theißen, G., Wong, G.K.-S., and One Thousand Plant Transcriptomes, I. (2019). One thousand plant transcriptomes and the phylogenomics of green plants. Nature **574,** 679-685.

Li, H., Handsaker, B., Wysoker, A., Fennell, T., Ruan, J., Homer, N., Marth, G., Abecasis, G., Durbin, R., and Genome Project Data Processing, S. (2009). The Sequence Alignment/Map format and SAMtools. Bioinformatics **25,** 2078-2079.

Li, L., Naseem, S., Sharma, S., and Konopka, J.B. (2015). Flavodoxin-like proteins protect *Candida albicans* from oxidative stress and promote virulence. PLOS Pathogens **11,** e1005147.

Liang, L., Liu, Y., Jariwala, J., Lynn, D.G., and Palmer, A.G. (2016). Detection and adaptation in parasitic angiosperm host selection. American Journal of Plant Sciences **7,** 1275-1290.

Lochner, K., Döring, O., and Böttger, M. (2003). Phylloquinone, what can we learn from plants? BioFactors **18,** 73-78.

Lohmann, A., Schottler, M.A., Brehelin, C., Kessler, F., Bock, R., Cahoon, E.B., and Dormann, P. (2006). Deficiency in phylloquinone (vitamin K1) methylation affects prenyl quinone distribution, photosystem I abundance and anthocyanin accumulation in the arabidopsis AtmenG mutant. Journal of Biological Chemistry **281,** 40461-40472.

Love, M.I., Huber, W., and Anders, S. (2014). Moderated estimation of fold change and dispersion for RNA-seq data with DESeq2. Genome Biology **15,** 550.

Lu, Y., Wang, H.-R., Li, H., Cui, H.-R., Feng, Y.-G., and Wang, X.-Y. (2013). A chloroplast membrane protein LTO1/AtVKOR involving in redox regulation and ROS homeostasis. Plant Cell Reports **32,** 1427-1440.

Luke, G.A., Roulston, C., Tilsner, J., and Ryan, M.D. (2015). Growing uses of 2A in plant biotechnology.

Lüthje, S., Döringe, O., and böttger, M. (1992). The effects of vitamin K3 and dicumarol on the plasma membrane redox system and h+ pumping activity of *Zea mays* L roots measured over a long time scale. Journal of Experimental Botany **43,** 183-188.

Lüthje, S., Van Gestelen, P., Córdoba-Pedregosa, M.C., González-Reyes, J.A., Asard, H., Villalba, J.M., and Böttger, M. (1998). Quinones in plant plasma membranes — a missing link? Protoplasma **205,** 43-51.

Margis, R., Dunand, C., Teixeira Felipe, K., and Margis-Pinheiro, M. (2008). Glutathione peroxidase family – an evolutionary overview. FEBS Journal **275,** 3959-3970.

Marmagne, A., Rouet, M.-A., Ferro, M., Rolland, N., Alcon, C., Joyard, J., Garin, J., Barbier-Brygoo, H., and Ephritikhine, G. (2004). Identification of new intrinsic proteins in *Arabidopsis* plasma membrane proteome. Molecular & Cellular Proteomics **3,** 675-691.

Martin, M. (2011). Cutadapt removes adapter sequences from high-throughput sequencing reads. EMBnet.journal **17,** 10-12.

Matvienko, M., Wojtowicz, A., Wrobel, R., Jamison, D., Goldwasser, Y., and Yoder, J.I. (2001). Quinone oxidoreductase message levels are differentially regulated in parasitic and non-parasitic plants exposed to allelopathic quinones. Plant Journal **25,** 375-387.

McNeal Joel, R., Bennett Jonathan, R., Wolfe Andrea, D., and Mathews, S. (2013). Phylogeny and origins of holoparasitism in Orobanchaceae. American Journal of Botany **100,** 971-983.

Michalecka, A.M., Svensson, Å.S., Johansson, F.I., Agius, S.C., Johanson, U., Brennicke, A., Binder, S., and Rasmusson, A.G. (2003). *Arabidopsis* genes encoding mitochondrial type II NAD(P)H dehydrogenases have different evolutionary origin and show distinct responses to light. Plant Physiology **133,** 642-652.

Mittler, R., Vanderauwera, S., Gollery, M., and Van Breusegem, F. (2004). Reactive oxygen gene network of plants. Trends in Plant Science **9,** 490-498.

Natera, S.H.A., Ford, K.L., Cassin, A.M., Patterson, J.H., Newbigin, E.J., and Bacic, A. (2008). Analysis of the *Oryza sativa* plasma membrane proteome using combined protein and peptide fractionation approaches in conjunction with mass spectrometry. Journal of Proteome Research **7,** 1159-1187.

Nelson, B.K., Cai, X., and Nebenführ, A. (2007). A multicolored set of *in vivo* organelle markers for co-localization studies in *Arabidopsis* and other plants. Plant Journal **51,** 1126-1136.

Nowicka, B., and Kruk, J. (2010). Occurrence, biosynthesis and function of isoprenoid quinones. Biochimica et Biophysica Acta (BBA) - Bioenergetics **1797,** 1587-1605.

Oostende, C.v., Widhalm, J.R., and Basset, G.J.C. (2008). Detection and quantification of vitamin K1 quinol in leaf tissues. Phytochemistry **69,** 2457-2462.

Palmer, C.M., and Guerinot, M.L. (2009). Facing the challenges of Cu, Fe and Zn homeostasis in plants. Nature Chemical Biology **5,** 333.

Pathi, K.M., Tula, S., and Tuteja, N. (2013). High frequency regeneration via direct somatic embryogenesis and efficient *Agrobacterium*-mediated genetic transformation of tobacco. Plant Signaling & Behavior **8,** e24354.

Patridge, E.V., and Ferry, J.G. (2006). WrbA from *Escherichia coli* and *Archaeoglobus fulgidus* is an NAD(P)H:quinone oxidoreductase. Journal of Bacteriology **188,** 3498.

Pechanova, O., Hsu, C.-Y., Adams, J.P., Pechan, T., Vandervelde, L., Drnevich, J., Jawdy, S., Adeli, A., Suttle, J.C., Lawrence, A.M., Tschaplinski, T.J., Séguin, A., and Yuceer, C. (2010). Apoplast proteome reveals that extracellular matrix contributes to multistress response in poplar. BMC Genomics **11,** 674-674.

Roberts, A., and Pachter, L. (2013). Streaming fragment assignment for real-time analysis of sequencing experiments. Nat Meth **10,** 71-73.

Ronquist, F., Teslenko, M., van der Mark, P., Ayres, D.L., Darling, A., Höhna, S., Larget, B., Liu, L., Suchard, M.A., and Huelsenbeck, J.P. (2012). MrBayes 3.2: Efficient Bayesian phylogenetic inference and model choice across a large model space. Systematic Biology **61,** 539-542.

Schopfer, P., Heyno, E., Drepper, F., and Krieger-Liszkay, A. (2008). Naphthoquinone-dependent generation of superoxide radicals by quinone reductase isolated from the plasma membrane of soybean. Plant Physiology **147,** 864-878.

Schultz, G., Soll, J., and Ellerbrock, B.H. (1981). Site of prenylation reaction in synthesis of phylloquinone (vitamin K1) by spinach chloroplasts. European Journal of Biochemistry **117,** 329-332.

Shannon, P., Markiel, A., Ozier, O., Baliga, N.S., Wang, J.T., Ramage, D., Amin, N., Schwikowski, B., and Ideker, T. (2003). Cytoscape: A software environment for integrated models of biomolecular interaction networks. Genome Research **13,** 2498-2504.

Small, I., Peeters, N., Legeai, F., and Lurin, C. (2004). Predotar: A tool for rapidly screening proteomes for N-terminal targeting sequences. PROTEOMICS **4,** 1581-1590.

Smith, C.E., Ruttledge, T., Zeng, Z., O'Malley, R.C., and Lynn, D.G. (1996). A mechanism for inducing plant development: the genesis of a specific inhibitor. Proceedings of the National Academy of Sciences **93,** 6986-6991.

Valentin, H.E., Lincoln, K., Moshiri, F., Jensen, P.K., Qi, Q., Venkatesh, T.V., Karunanandaa, B., Baszis, S.R., Norris, S.R., Savidge, B., Gruys, K.J., and Last, R.L. (2006). The *Arabidopsis* vitamin E pathway gene5-1 mutant reveals a critical role for phytol kinase in seed tocopherol biosynthesis. Plant Cell **18,** 212-224.

Veronesi, C., Bonnin, E., Calvez, S., Thalouarn, P., and Simier, P. (2007). Activity of secreted cell wall-modifying enzymes and expression of peroxidase-encoding gene following germination of *Orobanche ramosa*. Biologia Plantarum **51,** 391-394.

Wang, L., Li, Q., Zhang, A., Zhou, W., Jiang, R., Yang, Z., Yang, H., Qin, X., Ding, S., Lu, Q., Wen, X., and Lu, C. (2017). The phytol phosphorylation pathway is essential for the biosynthesis of phylloquinone, which is required for photosystem i stability in *Arabidopsis*. Molecular Plant **10,** 183-196.

Westwood, J.H., Yoder, J.I., Timko, M.P., and dePamphilis, C.W. (2010). The evolution of parasitism in plants. Trends in Plant Science **15,** 227-235.

Westwood, J.H., dePamphilis, C.W., Das, M., Fernández-Aparicio, M., Honaas, L.A., Timko, M.P., Wafula, E.K., Wickett, N.J., and Yoder, J.I. (2012). The Parasitic Plant Genome Project: New tools for understanding the biology of *Orobanche* and *Striga*. Weed Science **60,** 295-306.

Wrobel, R.L., Matvienko, M., and Yoder, J.I. (2002). Heterologous expression and biochemical characterization of an NAD(P)H:quinone oxidoreductase from the hemiparasitic plant *Triphysaria versicolor*. Plant Physiology and Biochemistry **40,** 265-272.

Yang, Z., Wafula, E.K., Honaas, L.A., Zhang, H., Das, M., Fernandez-Aparicio, M., Huang, K., Bandaranayake, P.C.G., Wu, B., Der, J.P., Clarke, C.R., Ralph, P.E., Landherr, L., Altman, N.S., Timko, M.P., Yoder, J.I., Westwood, J.H., and dePamphilis, C.W. (2015). Comparative transcriptome analyses reveal core parasitism genes and suggest gene duplication and repurposing as sources of structural novelty. Molecular Biology and Evolution **32,** 767-790.

Yoshida, S., Cui, S., Ichihashi, Y., and Shirasu, K. (2016). The haustorium, a specialized invasive organ in parasitic plants. Annual Review of Plant Biology **67,** 643-667.

Yoshida, S., Kim, S., Wafula, E.K., Tanskanen, J., Kim, Y.-M., Honaas, L., Yang, Z., Spallek, T., Conn, C.E., Ichihashi, Y., Cheong, K., Cui, S., Der, J.P., Gundlach, H.,

Jiao, Y., Hori, C., Ishida, J.K., Kasahara, H., Kiba, T., Kim, M.-S., Koo, N., Laohavisit, A., Lee, Y.-H., Lumba, S., McCourt, P., Mortimer, J.C., Mutuku, J.M., Nomura, T., Sasaki-Sekimoto, Y., Seto, Y., Wang, Y., Wakatake, T., Sakakibara, H., Demura, T., Yamaguchi, S., Yoneyama, K., Manabe, R.-i., Nelson, D.C., Schulman, A.H., Timko, M.P., dePamphilis, C.W., Choi, D., and Shirasu, K. (2019). Genome sequence of *Striga asiatica* provides insight into the evolution of plant parasitism. Current Biology **29,** 3041-3052.e3044.

Zhang, W., Liu, T., Ren, G., Hörtensteiner, S., Zhou, Y., Cahoon, E.B., and Zhang, C. (2014). Chlorophyll degradation: The tocopherol biosynthesis-related phytol hydrolase in *Arabidopsis* seeds is still missing. Plant Physiology **166,** 70.

Figure legends

Figure 1. Phylloquinone biosynthesis in parasitic plants.

(A) A simplified phylloquinone biosynthetic pathway from top to bottom as numbered and color-coded by their predicted subcellular localization.

(B) Expression profiles of phylloquinone genes during parasitic plant development. Gene order is the same as in (A), and Y-axis is shown on the right. Developmental stages are as reported (Yang et al., 2015): 0, imbibed seeds; 1, germinated seeds/radicles; 2, HIF-treated seedlings; 3, haustoria, pre-vascular connection; 4.1, haustoria, post-vascular connection; 6.1, leaves/stems; 6.2, floral buds. Data from alternative gene candidates for the penultimate step are shown on the lower right panels, with grey dashed/dotted lines denoting the scale.

(C) HPLC detection of phylloquinone in germinated *P. aegyptiaca* seeds (top panel), and with spiked authentic standard (lower panel). Menaquinone (MK-4) was included as a reference.

(D) HPLC detection of phylloquinone in *A. thaliana* seed (top panel), with authentic standard (lower panel).

Figure 2. Characterization of MenA and MenG.

(A) Plastid-targeting prediction of MenA and MenG polypeptides from various species. Heatmaps show prediction strengths above the 50th percentile of each method. Those with a high prediction score from at least one program are deemed potentially plastidial, as not all methods accurately predict experimentally characterized plastidial proteins (asterisks). Introns are not drawn to scale.

(B) Transmembrane domain prediction of AtMenA (green line denoting the transit peptide) and
910 PaMenA2 (shifted x-axis for domain alignment).
(C-D) Confocal images of PaMenA2-GFP (C) and PaMenG2-GFP (D) colocalization with a
912 plasma membrane marker AtPIP2A-mCherry. Scale bars = 20 µm.
(E) HPLC analysis of *E. coli* ΔmenG mutant strain JW5581 expressing *PaMenG2* or the
914 *EcMenG* control. (D)MK-8, (demethyl)menaquinone-8.
(F-G) Bayesian phylogeny of MenA and MenG from representative Asterids and two Rosids. At,
916 *Arabidopsis thaliana*; Ca, *Conopholis americana*; Lp, *Lindenbergia philippensis*; Migut,
Mimulus guttatus; Of, *Orobanche fasciculata*; Pa, *Phelipanche aegyptiaca*; Potri, *Populus*
918 *trichocarpa*; Rg, *Rehmannia glutinosa*; Solyc, *Solanum lycopersicum*; Sh, *Striga hermonthica*;
Tv, *Triphysaria versicolor*; Vt, *Verbascum thapsus*. Branch support is shown for major nodes.
920

Figure 3. Coexpression of phylloquinone genes.
922 (A-F) Coexpression patterns among phylloquinone biosynthetic genes, including multifunctional
NDC1 and *QR2*, based on Gini correlation coefficient. Relevant genes or gene members involved
924 in phylloquinone biosynthesis are boxed. The exceptions are *A. thaliana AtICSs* involved in
salicylic acid biosynthesis for defense and *AtDHNATs* in peroxisomal β-oxidation (dashed box),
926 besides phylloquinone biosynthesis. The corresponding *Arabidopsis*, *Glycine* and *Populus* gene
models are shown on the x-axis with shortened prefix for soybean (Gm = Glyma) and poplar (Pt
928 = Potri).
(G) GO enrichments of phylloquinone-coexpressed genes defined as the union set of the top 500
930 most highly-correlated transcripts for each phylloquinone gene. Only the top 10 categories are
shown. Similar results were obtained using Gini correlation coefficient ≥0.8 to extract
932 phylloquinone-coexpressed genes.

934 **Figure 4. Phylloquinone gene coexpression networks.**
(A) Network visualization of the three parasitic plants. Edge thickness reflects the coexpression
936 strength. Key gene nodes are color-coded by pathway or family, and *QR2* is colored differently
from the other phylloquinone genes (*NDC1* was not captured in any of the networks). Horizontal
938 bars depict the distribution of nodes according to their connectivity with phylloquinone genes
(k_{PhQ}).

940 (B) Bayesian phylogeny of peroxidases (PRX). Orthologs of experimentally characterized PRXs
are color-coded by species in the blue clade.
942 (C-F) Expression profiles of *PRX* (C), *FRO1/NOX1* (D), *CSD1* (E), and *GPX4* (F) orthologs.
Solid symbols denote phylloquinone-coexpressed genes ($k_{PhQ} \geq 3$), and others are shown in open
944 symbols. Developmental stages are the same as in Figure 1.

946 **Figure 5. Evolutionary changes in subcellular localization of phylloquinone biosynthesis.**
Conserved early- and mid-pathway steps are shown as circled numbers (1-7, see Figure 1) and
948 late pathway steps MenA and MenG are abbreviated as A1/A2 and G1/G2, respectively. Circle
colors denote different subcellular compartments: green, plastid; orange, peroxisome (px);
950 purple, plasma membrane (PM). Branches of the simplified eudicot phylogeny in the middle
point to corresponding illustrations of changing pathway organization with representative species
952 indicated. Clockwise from lower left, exclusively plastidial late steps in rosids and some asterids
such as solanales; top left, dual plastidial and plasma membrane targeting in certain
954 photosynthetic Orobanchaceae, attributable to lamiale-specific duplication of MenA and MenG.
Differential losses of *MenA* and *MenG* genes in other photosynthetic, hemiparasitic (top right)
956 and holoparasitic (lower right) lineages, with the latter exclusively PM targeting. pg,
plastoglobules.

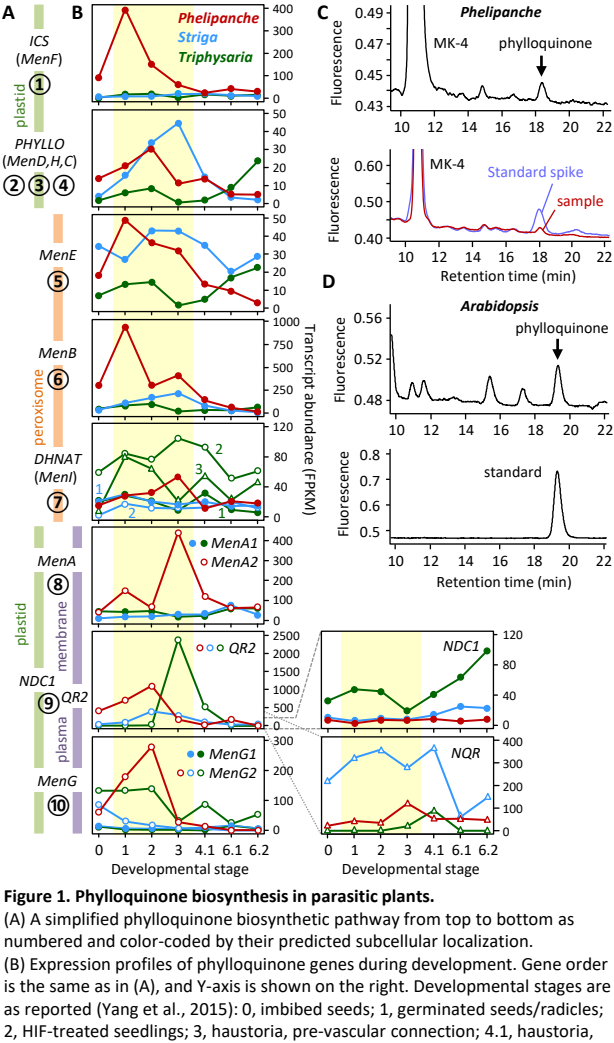

Figure 1. Phylloquinone biosynthesis in parasitic plants.

(A) A simplified phylloquinone biosynthetic pathway from top to bottom as numbered and color-coded by their predicted subcellular localization.

(B) Expression profiles of phylloquinone genes during development. Gene order is the same as in (A), and Y-axis is shown on the right. Developmental stages are as reported (Yang et al., 2015): 0, imbibed seeds; 1, germinated seeds/radicles; 2, HIF-treated seedlings; 3, haustoria, pre-vascular connection; 4.1, haustoria, post-vascular connection; 6.1, leaves/stems; 6.2, floral buds. Data from alternative gene candidates for the penultimate step are shown on the lower right panels, with grey dashed/dotted lines denoting the scale. Different DHNAT genes are denoted by numbers (1/2/3 = DHNAT1/2/3)

(C) HPLC detection of phylloquinone in germinated P. aegyptiaca seeds (top panel), and with spiked authentic standard (lower panel). Menaquinone (MK-4) was included as a reference.

(D) HPLC detection of phylloquinone in A. thaliana seed (top panel), with authentic standard (lower panel).

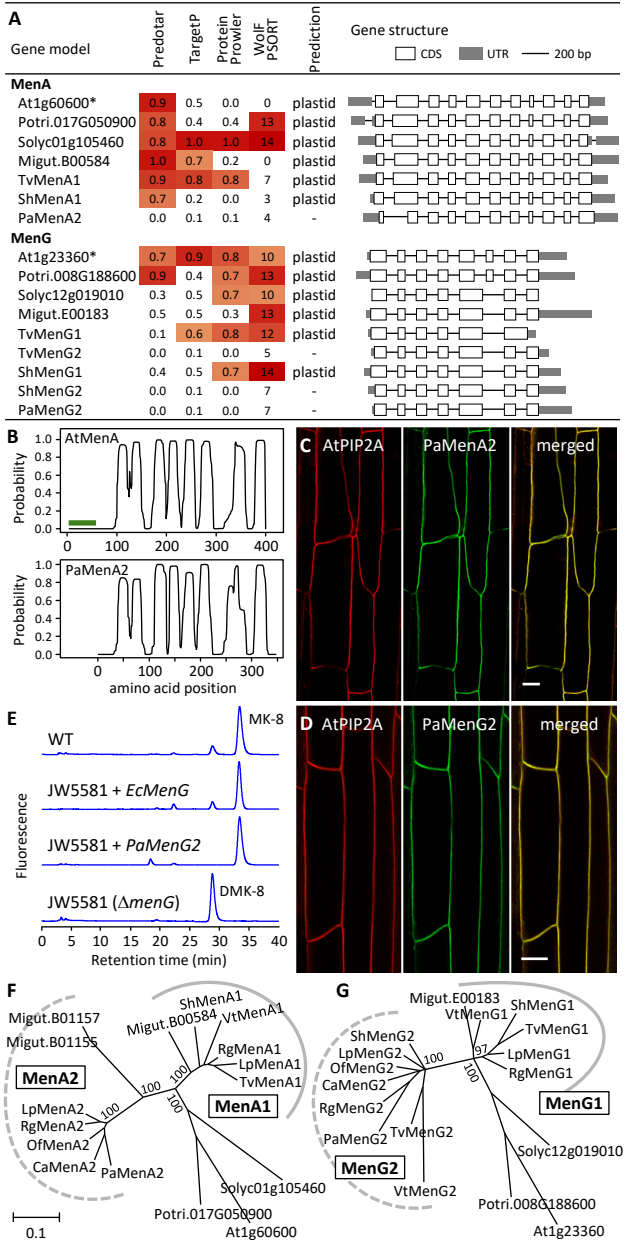

Figure 2. Characterization of MenA and MenG.
(A) Plastid-targeting prediction of MenA and MenG polypeptides from various species. Heatmaps show prediction strengths above the 50th percentile of each method. Those with a high prediction score from at least one program are deemed plastidial, as not all methods accurately predict experimentally characterized plastidial proteins (asterisks). Introns are not drawn to scale.
(B) Transmembrane domain prediction of AtMenA (green line denoting the transit peptide) and PaMenA2 (shifted x-axis for domain alignment).
(C-D) Confocal images of PaMenA2-GFP (C) and PaMenG2-GFP (D) colocalization with a plasma membrane marker AtPIP2A-mCherry. Scale bars = 20 µm.
(E) HPLC analysis of *E. coli* ΔmenG mutant strain JW5581 expressing *PaMenG2* or the *EcMenG* control. (D)MK-8, (demethyl)menaquinone-8.
(F-G) Bayesian phylogeny of MenA and MenG from representative Asterids and two Rosids. At, *Arabidopsis thaliana*; Ca, *Conopholis americana*; Lp, *Lindenbergia philippensis*; Migut, *Mimulus guttatus*; Of, *Orobanche fasciculata*; Pa, *Phelipanche aegyptiaca*; Potri, *Populus trichocarpa*; Rg, *Rehmannia glutinosa*; Solyc, *Solanum lycopersicum*; Sh, *Striga hermonthica*; Tv, *Triphysaria versicolor*; Vt, *Verbascum thapsus*. Branch support is shown for major nodes.

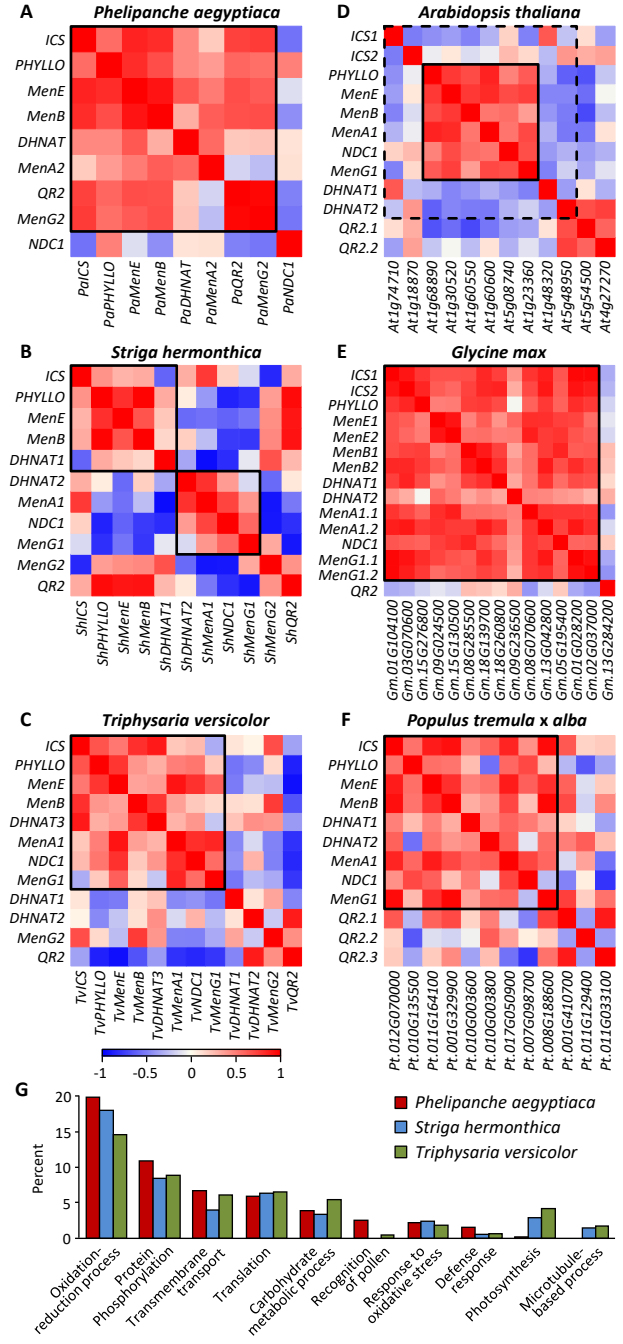

Figure 3. Coexpression of phylloquinone genes.

(A-F) Coexpression patterns among phylloquinone biosynthetic genes, including multifunctional *NDC1* and *QR2*, based on Gini correlation coefficient. Relevant genes or gene members involved in phylloquinone biosynthesis are boxed. The exceptions are *A. thaliana AtICSs* involved in salicylic acid biosynthesis for defense and *AtDHNATs* in peroxisomal β-oxidation (dashed box), besides phylloquinone biosynthesis. The corresponding *Arabidopsis*, *Glycine* and *Populus* gene models are shown on the x-axis with shortened prefix for soybean (Gm = Glyma) and poplar (Pt = Potri).

(G) GO enrichments of phylloquinone-coexpressed genes defined as the union set of the top 500 most highly-correlated transcripts for each phylloquinone gene. Only the top 10 categories are shown. Similar results were obtained using Gini correlation coefficient ≥0.8 to extract phylloquinone-coexpressed genes.

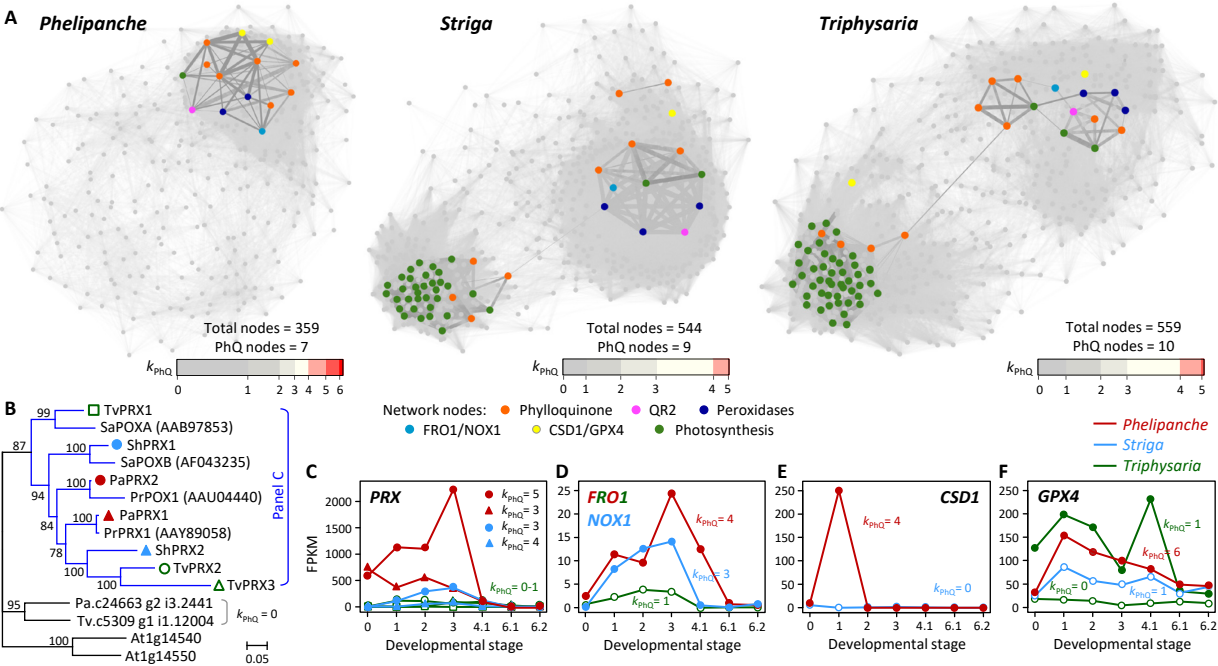

Figure 4. Phylloquinone gene coexpression networks.

(A) Network visualization of the three parasitic plants. Edge thickness reflects the coexpression strength. Key gene nodes are color-coded by pathway or family, and *QR2* is colored differently from the other phylloquinone genes (*NDC1* was not captured in any of the networks). Horizontal bars depict the distribution of nodes according to their connectivity with phylloquinone genes (k_{PhQ}).

(B) Bayesian phylogeny of peroxidases (PRX). Orthologs of experimentally characterized PRXs are color-coded by species in the blue clade.

(C-F) Expression profiles of *PRX* (C), *FRO1/NOX1* (D), *CSD1* (E), and *GPX4* (F) orthologs. Solid symbols denote phylloquinone-coexpressed genes ($k_{PhQ} \geq 3$), and others are shown in open symbols. Developmental stages are the same as in Figure 1.

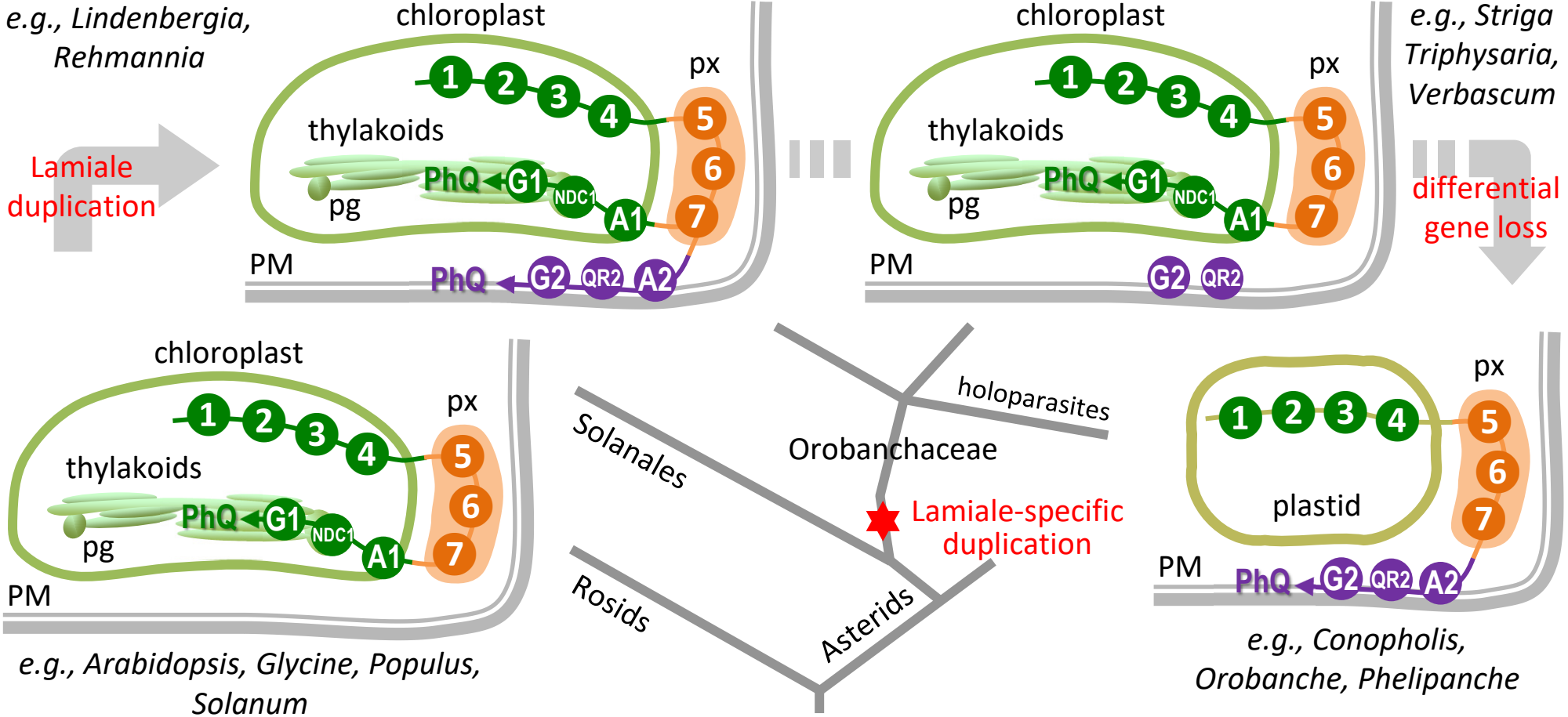

Figure 5. Evolutionary changes in subcellular localization of phylloquinone biosynthesis. Conserved early- and mid-pathway steps are shown as circled numbers (1-7, see Figure 1) and late pathway steps MenA and MenG are abbreviated as A1/A2 and G1/G2, respectively. Circle colors denote different subcellular compartments: green, plastid; orange, peroxisome (px); purple, plasma membrane (PM). Branches of the simplified eudicot phylogeny in the middle point to corresponding illustrations of changing pathway organization with representative species indicated. Clockwise from lower left, exclusively plastidial late steps in rosids and some asterids such as solanales; top left, dual plastidial and PM targeting in certain photosynthetic Orobanchaceae attributable to lamiale-specific duplication of MenA and MenG. Differential losses of *MenA* and *MenG* genes in other photosynthetic, hemiparasitic (top right) and holoparasitic (lower right) lineages, with the latter exclusively PM targeting. pg, plastoglobules.